Vacancies, Interstitials, and Rare Gases in Fluorite Structures

S. C. Keeton and W. D. Wilson
Physical Research Division I and II, Sandia Laboratories, Livermore, California 94550
(Received 31 August 1972)

We have calculated the Ca^{++}-F^-, Ba^{++}-F^-, Ca^{++}-Ca^{++}, Ba^{++}-Ba^{++}, and F^--F^- interatomic potentials using a semiclassical method. Using these potentials, the anion vacancy and interstitial formation and activation energies were determined. Franklin's potentials were also employed for comparison. The results are in excellent agreement with experiment for BaF_2 and for most of the CaF_2 results. The unusually wide range (0.53–1.65 eV) of experimental values for interstitial-related activation energies makes this direct comparison in CaF_2 difficult, but our results clearly indicate the interstitialcy mechanism of anion interstitial migration to be dominant in both CaF_2 and BaF_2. Using the same method, the energies of formation of He, Ne, and Ar at interstitial sites in CaF_2 were determined to be 0.49, 1.59, and 3.08 eV, respectively. The activation energy for interstitial motion of these atoms was found to be ≈ 1.4 eV for all three gases. Furthermore, we find it takes 0.25, 0.95, and 2.30 eV to place a He, Ne, or Ar gas atom, respectively, in an existing anion vacancy. The substitutional detrapping energy, the energy required to move a rare-gas atom from an anion vacancy to its nearest-neighbor stable interstitial position, was found to be 1.8, 2.1, and 2.5 eV for He, Ne, and Ar, respectively. The explicit atomistic calculation is done for many regions of varying size surrounding each defect so that it is possible to say, at least semiquantitatively, that the energy vs radius of the region r_A varies as $1/r_A$ for charged defects and as $1/r_A^2$ for neutral defects.

I. INTRODUCTION

There has been a continuing experimental effort involved in the understanding of the basic defect properties of fluorite crystals. Ionic conductivity, dielectric loss, and NMR measurements have been performed on pure and impurity-doped crystals primarily to determine the formation and activation energies of vacancies and interstitials in these substances.[1–22] In attempting to predict these formation and activation energies, most of the theoretical calculations[23–27] have explicitly treated the interactions of only a few atoms near the defect and accounted for the remainder of the crystal by a continuum approximation. We show here that one must include explicitly the interactions of about 100 atoms nearest to the defect before employing a continuum technique, in order to account for ionic relaxations which depend on the defect symmetry and would not be accounted for properly by a continuum technique. All of the previous theoretical calculations referenced have utilized Born–Mayer repulsive potentials for the Ca^{++} and F^- ions comprising the lattice.

There have also been a number of experimental investigations of the diffusion of rare gases in CaF_2.[28–37] The purpose of these experiments was to simulate rare-gas diffusion in UO_2 reactor fuel elements (CaF_2 having the same crystal structure as UO_2); thus most of the measurements have involved fast-neutron irradiation of pure or doped CaF_2. The Ar atoms (or other rare-gas atoms such as Xe created as a fission product from impurities doped into CaF_2) so created diffuse through the lattice and are detected by gas-release techniques. Interpretation of the data is complicated by the radiation damage which may give rise to traps for the rare-gas atoms, thus giving higher values for the Ar-diffusion activation energy than would be characteristic of the undamaged bulk crystal. Norgett[27] has calculated the activation energy for a single Ar atom moving via an interstitial mechanism in CaF_2 using a modified Mott–Littleton method together with Born–Mayer repulsive potentials, including a van der Waals term, for the atomic constituents and Ar. In his calculations he treats explicitly the interactions of over 100 atoms near the defects considered.

A major difficulty with Born–Mayer potentials is that they are obtained from crystal data and hence are known only in the neighborhood of the equilibrium interatomic separation. A recent semiclassical treatment of two-body repulsive interactions enables one to readily determine the energy versus distance curve for any separation.[38,39] In this paper, the method is applied to the calculation of Ca^{++}-F^-, Ba^{++}-F^-, F^--F^-, Ca^{++}-Ca^{++}, Ba^{++}-Ba^{++}, Ca^{++}-(rare gas)^0, and F^--(rare gas)^0 interactions. These potentials are then employed in the determination of the formation and activation energies of defect complexes in CaF_2 and BaF_2.

In Sec. II, the repulsive interactions are given and compared with those of Franklin.[25,26] Section II also contains a brief description of the method of calculation of the defect properties. In Sec. III, the CaF_2 and BaF_2 results and a discussion thereof is presented.

II. ENERGY TERMS

It has been established experimentally that the binding in CaF_2 and BaF_2 crystals is largely ionic.[40] In such a crystal, the ions can be considered to

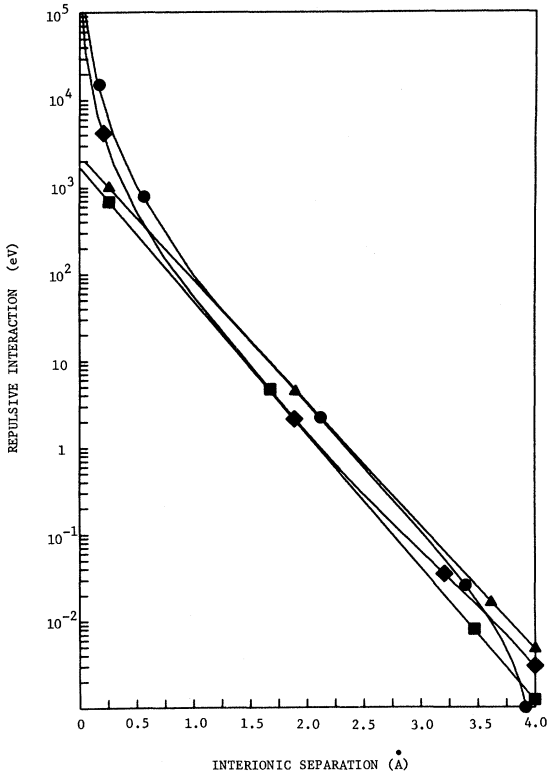

FIG. 1. Repulsive potentials for cation-anion interactions in BaF_2 and CaF_2: • $Ba^{++}-F^-$ from semiclassical method; ▲ $Ba^{++}-F^-$ from Franklin (Ref. 26); ◆ $Ca^{++}-F^-$ from semiclassical method; ■ $Ca^{++}-F^-$ from Franklin (Ref. 25).

be free ions for the purpose of calculating the repulsive interactions between constituents. Following Wilson and Bisson,[39] the Ca^{++}, Ba^{++}, and F^- charge distributions were obtained in the Hartree–Fock–Slater approximation. Two-body interactions between these ions are calculated using the Wedepohl method.[38,39] These calculated potentials for CaF_2 and BaF_2 shall collectively be denoted potentials I and III, respectively. In addition, the Born–Mayer potentials of Franklin[25,26] were used; for CaF_2 his set number 3 potentials[25] shall be called potential II and for BaF_2 his set number 2 potentials[26] shall be called potential IV.

In Fig. 1, the $Ca^{++}-F^-$ and $Ba^{++}-F^-$ interactions are plotted and compared with those obtained by Franklin. The agreement with Franklin's CaF_2 and BaF_2 potentials in the vicinity of the interatomic separations r_0 ($r_0 = 2.36$ Å and 2.68 Å, respectively) is quite striking in light of the fact that no empirical data were employed in this calculation. If one piecewise fits exponentials in various regions of interatomic separation, one obtains the Born–Mayer parameter values given in Table I. The agreement with Franklin's results for both CaF_2 and BaF_2 (which were fit to experimental data) is best in a region somewhat short of the equilibrium interatomic separation. Actually, the A_{+-} and ρ_{+-} values reported by Franklin as set number 1 for CaF_2 (1477 eV and 0.289 Å, respectively) are in better agreement with the values determined by our method for the 2.0–2.5-Å region. There is, in general, a gradual increase in the (negative) slope of our potential as r increases until the potential actually goes slightly negative by ~0.001 eV exhibiting a well-like behavior (not shown in Fig. 1). This is a consequence of the classical nature of the potential as discussed by Wedepohl[38] and is not physically realistic. As a result, in the actual defect calculations the potential was truncated at a value $\sim 10^{-4}$ eV, which was considered zero for all practical purposes.

In Fig. 2, the F^-F^- interaction is plotted and compared with those of Franklin; the corresponding piecewise Born–Mayer parameters are given in Table I. The F^-F^- separation in CaF_2 is 2.73 Å, and in that vicinity the calculated repulsive interaction energy is decreasing rapidly with increasing distance. This was felt to be of possible importance to the defect properties and therefore several variations were tried. We performed nearly all of the formation and activation energy calculations using potential I not only with the semiclassical F^-F^- potential plotted in Fig. 2 but with this F^--

TABLE I. Comparison of Born–Mayer parameters obtained by piecewise fitting of the calculated semiclassical potentials to the form $A_{ij}e^{-r_{ij}/\rho_{ij}}$ in the regions indicated, to existing values. Parameters A_{ij} are given in eV and the ρ_{ij} are in Å.

	$Ca^{++}-F^-$		F^-F^-		$Ba^{++}-F^-$	
Range (Å)	A_{+-}	ρ_{+-}	A_{--}	ρ_{--}	A_{+-}	ρ_{+-}
1.0–1.5	2267	0.2710	1178	0.2731	3353	0.2841
1.5–2.0	1986	0.2777	1102	0.2765	2568	0.2992
1.75–2.0	1713	0.2835			2707	0.2968
2.0–2.5	1042	0.3050	1898	0.2572	2900	0.2938
2.5–3.0	537	0.3318			2878	0.2941
3.0–3.5	423	0.3409			9780	0.2626
3.5–4.0	1036	0.3135			1009	0.3165
Norgett[a]	2914	0.2705	721.3	0.2705		
Ra[b]	2947	0.274	306.6	0.357	3228	0.310
			(128.2)[c]	(0.367)[c]		
Franklin[a]	1714	0.2820	457	0.2820	2340	0.305
			(209)[c]	(0.305)[c]		

[a]Born–Mayer parameters apply for all separation values from Franklin CaF_2 (Refs. 25 and 26) and BaF_2 (Ref. 26); from Norgett (Ref. 27).

[b]ρ parameters determined quantum mechanically from overlap integrals; A parameters fitted to experimental data (Ref. 48).

[c]Ra[48] and Franklin[25,26] each give different F^-F^- parameters for CaF_2 and BaF_2; values for BaF_2 are in parenthesis.

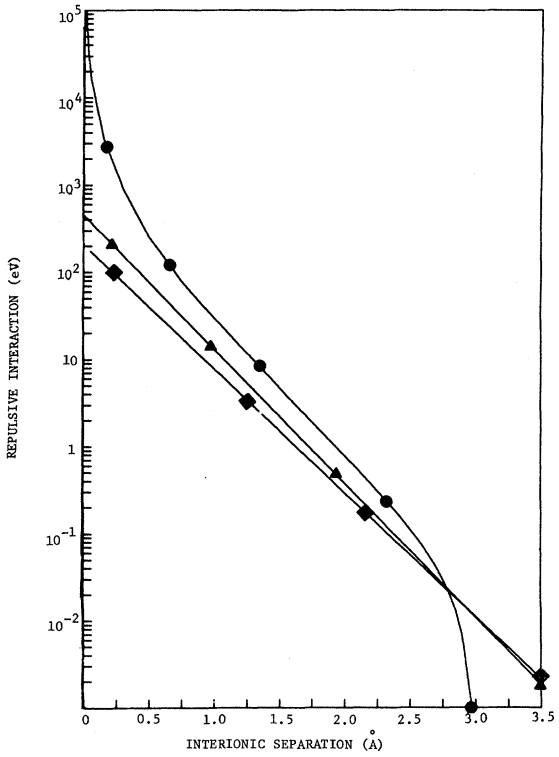

FIG. 2. Repulsive potentials for F^--F^- interactions in BaF_2 and CaF_2. • CaF_2 and BaF_2 from semiclassical method; ◆ BaF_2 from Franklin (Ref. 25); ▲ CaF_2 from Franklin (Ref. 26).

F^- potential exponentially extended beyond 2.0 Å (with Born–Mayer parameters $A_{--} = 1173$ eV, $\rho_{--} = 0.2741$ Å) and also with the CaF_2 Franklin potential for F^--F^-. Neither of these variations changed the formation energy by more than ~0.1 eV. All pairwise potentials calculated using the Wedepohl method give the correct $1/R$-like behavior at small separations as the nuclear-nuclear repulsion begins to dominate.

In Figs. 3 and 4 are given the repulsive interactions between rare gases and Ca^{++} and F^-, respectively, determined by the Wedepohl method. These potentials were then employed with both potentials I and II in the calculation of several rare-gas defect complexes in CaF_2. (When referring to the rare-gas defect calculations, potential I and potential II will be used to denote the composite potentials corresponding to potential I and potential II, respectively, plus the rare-gas–lattice-ion potentials.)

In addition to the repulsive energy contribution to the formation of a defect the electrostatic and electronic polarization energy contributions were also included. Ewald sums were obtained using standard techniques[41] and the electronic polarization energy was calculated using the method originally due to Hatcher and Dienes.[42,43] The polarizabilities employed were 0.98, 2.42, and 0.76 Å^3 for Ca^{++}, Ba^{++}, and F^-, respectively.[25,44] The rare-gas polarizabilities used were 0.205, 0.395, and 1.642 Å^3 for He, Ne, and Ar, respectively.[45]

Quigley and Das[46] have suggested that the polarizability of an ion should decrease linearly with distance from its neighbors in a crystal, owing to overlap of electronic shells. In all calculations we calculated the electronic polarization energy both varying the anion polarizability in this way and keeping the anion polarizability fixed at 0.76 Å^3; the resulting differences in the formation energies were typically less than 0.1 eV. The energies reported are those obtained by allowing the anion polarizability to vary as this seemed more physically realistic.

An approximation to the total polarization energy (ionic plus electronic) can be obtained by an early method due to Jost.[47] Such continuum methods have the advantage of being analytic and easily evaluated but do not properly take into account the symmetry of the defect—a most important consideration because ionic relaxations associated with a particular defect are not isotropic. For neutral defects, such as rare-gas interstitials, long-range polarization effects do not exist and the calculation can be done

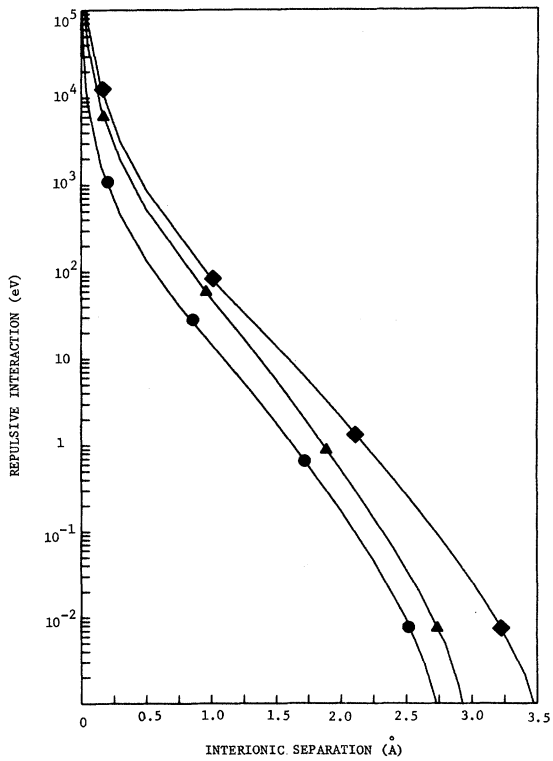

FIG. 3. Repulsive potentials for (rare gas)^0-Ca^{++} interactions from semiclassical method: • He-Ca^{++}; ▲ Ne-Ca^{++}; ◆ Ar-Ca^{++}.

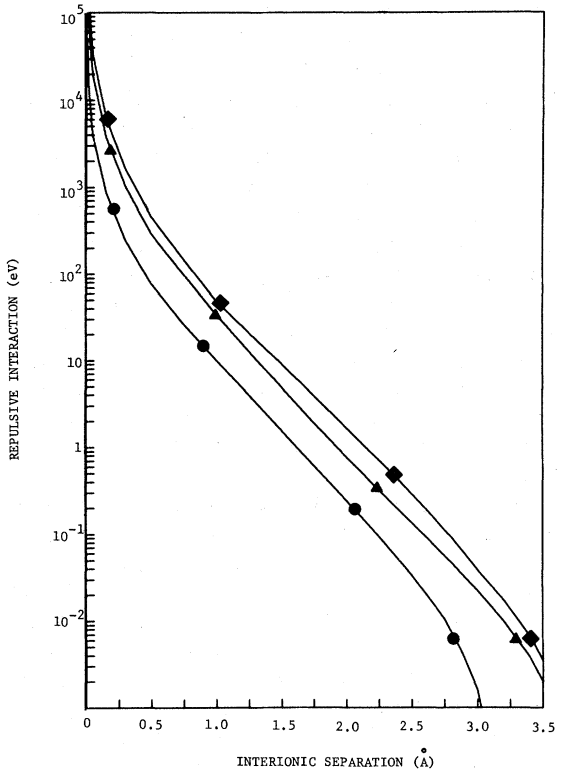

FIG. 4. Repulsive potentials for (rare gas)^0–F^- interactions from semiclassical method: ● He-F^-; ▲ Ne-F^-; ◆ Ar-F^-.

completely atomistically to the accuracy required for this work. Charged defects, however, introduce long-range effects which must be treated approximately. We therefore calculated the formation energy of a charged defect by explicitly treating all interactions within a "spherical" region (region A) of radius r_A surrounding the defect (up to 596 atoms included) and accounted for the remaining atoms in the crystal by an extrapolation technique to be described in the next section. For comparison we accounted for the remaining atoms with a Jost continuum. The accuracy of both approximations clearly depends upon the size of region A; and the results of this study are presented in Sec. III. All coordinates given are with respect to an F^- at the origin.

III. RESULTS AND DISCUSSION

A. Anion Formation and Migration Energies in CaF_2 and BaF_2

As described earlier, the formation energy of a defect is taken to be the sum of the explicitly calculated repulsive, electrostatic and polarization energies of the atoms in regions A, E_A, and the continuum energy w of the atoms outside A. A simple approximation to this energy was very early given by Jost, [47]

$$w = (q^2/2r_A)\,(1 - 1/k), \tag{1}$$

where q is the charge of the defect and k the low-frequency dielectric constant ($k = 6.76$ for CaF_2, $k = 7.33$ for BaF_2).

Motivated by this, we have plotted in Fig. 5 the atomistically calculated E_A vs $1/r_A$ for an anion vacancy in BaF_2 using both potentials III and IV. One notes that beyond a value of r_0/r_A of $\frac{1}{3}$ ($r_A \sim 8.0$ Å) corresponding to 124 atoms, the E_A values lie on a straight line, demonstrating the fundamen-

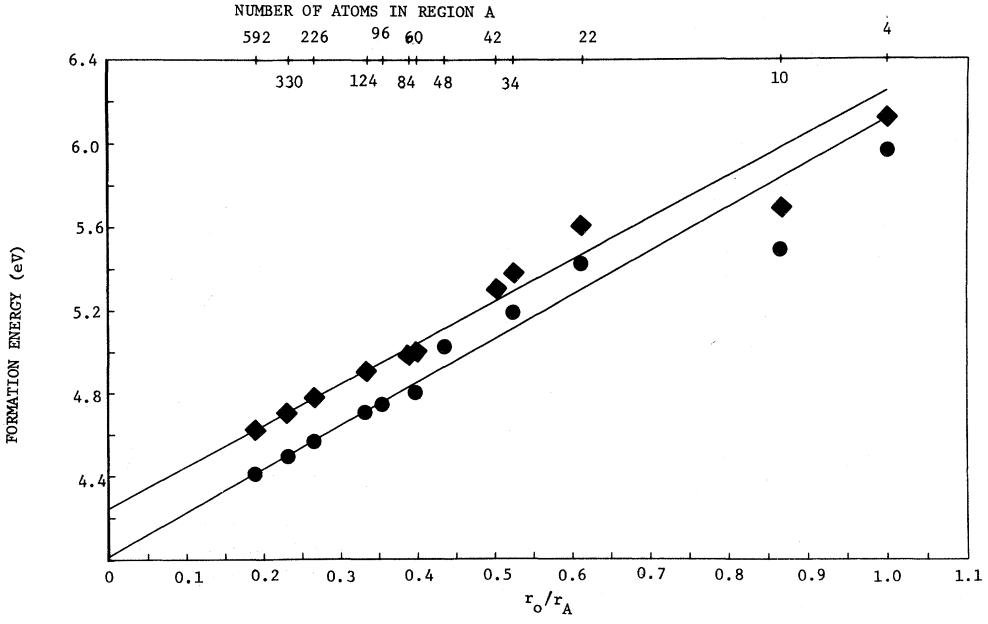

FIG. 5. Dependence of formation energy in eV on radius r_A of region A for an F^- vacancy in BaF_2. Straight line obtained from least-squares fit to energy values weighted by corresponding number of ions included in region A and are given at top of graph: ◆ using potential III; ● using potential IV.

tal correctness of the continuum approach in regions far from the defect. The straight line was determined by a least-squares fit of the calculated energies with each point weighted by the number of ions included, and is the weighting procedure used in all of these calculations. The slopes of these lines are 5.21 and 5.81 eV/Å^{-1} for potentials III and IV, respectively, which are each within about 15% of the 6.12 eV/Å^{-1} slope determined using the Jost Eq. (1) directly. The extrapolation of the straight lines in Fig. 5 to $r_A^{-1}=0$ gives energies of 4.25 and 4.00 eV for potentials III and IV, respectively, or ~0.5 eV below the values which would be obtained from the largest region employed alone containing 592 atoms, $r_0/r_A=0.19$ ($r_A\sim 14.1$ Å). Adding the value from Eq. (1) with $r_0/r_A=0.19$ (see Table II for appropriate r_0's) to the calculated formation energy for a region A containing 592 atoms gives a formation energy of 4.18 and 3.97 eV for potentials III and IV, respectively, in excellent agreement with the more exact values obtained by extrapolation. In all the charged defect calculations which follow, the formation energies were determined in two ways; by an $r_A^{-1}=0$ extrapolation from a least-squares straight-line fit to several (nine or more, in general) calculated values of E_A vs r_A^{-1} (as in Fig. 5) and by adding the Jost value from Eq. (1) to the E_A number calculated for the largest region A. The formation energies arrived at using the two techniques generally were within 0.05 eV of one another; however, for the interstitial saddle point and interstitialcy saddle point they differed by as much as several tenths of an eV because the slope of the best straight line was 30–50% greater than the slope derived from Eq. (1).

For potential I, region A was restricted to 126 atoms for all defects because of convergence problems. It seems that the inclusion of more than about 150 ions in region A leads to a polarization catastrophe when potential I is employed. Since we have not included higher-order terms such as distortion dipoles, etc., it is not clear whether the difficulty lies with the repulsive interaction or with the point-dipole approximation. The above problem was not encountered with potentials II, III, or IV. For up to about 126 atoms potential I produced defect energies which follow the same behavior as a function of r_A as those yielded by the other potentials, e.g., see Figs. 6–8 in Sec. III B on rare-gas defects. We feel, therefore, that the inclusion of up to about 126 atoms results in meaningful defect energies for potential I. However, because of this occurrence the results obtained for CaF_2 using potential II (Franklin's host atom potential together with the Wedepohl potentials for the rare-gas interactions) will be stressed in what follows.

In Table II, the calculated lattice energies, interatomic separations, and anion vacancy and in-

TABLE II. Calculated lattice energies, interatomic separations, and formation energies of anion vacancies and interstitials in CaF_2 and BaF_2.

	CaF_2 Present work				BaF_2 Present work			
	Potential I[a]	Potential II[b]	Expt.	Other theory[c]	Potential III[a]	Potential IV[b]	Expt.	Other theory[d]
Lattice energy, eV	26.94	27.35	27.04[e]	27.28–27.35	24.58	24.16[e]	24.16[e]	23.9
Interatomic separation r_0, Å	2.36	2.34	2.36[f]	2.35	2.62	2.66	2.68[f]	theory[d]
F^- vacancy formation energy, eV	3.49	4.15		4.38–4.63	4.25	4.00		4.2
F^- interstitial formation energy, eV	−1.75	−2.10		−2.41–−1.77	−2.30	−2.15		−1.9
Anion Frenkel pair-formation energy, eV	1.74	2.05	2.2–[g] 3.1	2.11–2.75	1.95	1.85	1.9[h]	2.3

[a]Semiclassical potentials calculated here.
[b]Franklin potentials, set number 3 for CaF_2 (Ref. 25) and, set number 2 for BaF_2 (Ref. 26).
[c]Franklin (Ref. 25), Tharmalingam (Ref. 23), and Norgett (Ref. 27).
[d]Franklin (Ref. 26).
[e]Brackett and Brackett (Ref. 49).
[f]Wyckoff (Ref. 50).
[g]Ure (Ref. 18), Fielder (Ref. 9), Barsis and Taylor (Ref. 13), Bollman *et al.* (Ref. 19), Ratnam (Ref. 22), and H. Matzke (Ref. 2).
[h]Barsis and Taylor (Ref. 7).

TABLE III. Anion migration energies in CaF_2 and BaF_2.[a]

	CaF_2 Present work				BaF_2 Present work		
	Potential I	Potential II	Expt.	Other theory[b]	Potential III	Potential IV	Expt.
F^- vacancy activation, eV	0.3	0.4	0.36–1.21[c]	0.31–0.64	0.4	0.4	0.56[d]
F^- interstitial activation, eV	1.3	1.5		2.08–2.52	2.3	1.6	
F^- interstitialcy activation, eV	0.6	0.7	0.53–1.65[e]	1.29–1.56	0.8	0.7	0.79[f]

[a]The vacancy saddle point was $(\frac{1}{4}, 0, \frac{1}{4})$, the interstitial saddle point was $(\frac{1}{4}, \frac{1}{4}, \frac{1}{2})$, and the interstitialcy saddle point (0.075, 0.075, 0.370).

[b]For several different potentials, Chakravorty (Ref. 24)

[c]Ure (Ref. 18), Barsis and Taylor (Ref. 13), Lysiak and Mahendroo (Ref. 14), Fielder (Ref. 9), Rossing (Ref. 15), Champion (Ref. 17), Clark and Warren (Ref. 16), Bollman *et al.* (Ref. 19), Keig and Coble (Ref. 20), and Asadi (Ref. 21).

[d]Barsis and Taylor (Ref. 7).

[e]Ure (Ref. 18), Twidell (Ref. 1), Lysiak and Mahendroo (Ref. 14), Southgate (Ref. 12), Chen and McDonough (Ref. 4), Rossing (Ref. 15), Nikitinskaya *et al.* (Ref. 5), Popov, (Ref. 3), Fong and Hiller (Ref. 8), and Bollman *et al.* (Ref. 19).

[f]Barsis and Taylor (Ref. 6).

terstitial formation energies are given for both CaF_2 and BaF_2 and compared with the results of other workers. Up to 592 (596) ions were included in region A for the vacancy (interstitial) calculations. The excellent agreement between theory and experiment for the lattice energy and interatomic separation is due to the fact that the Coulomb contribution to the total energy dominates in an ionic solid, making these quantities rather insensitive to the repulsive potentials. Furthermore, potentials II and IV were fitted to the interatomic separation (but not the lattice energy).

Note that we obtained a somewhat lower energy for anion vacancy formation energy in CaF_2 than did Franklin using the same repulsive potential (potential II). This is likely to be the result of our using a larger region A, out to 46 neighbors or 592 ions to the defect, than did Franklin who only included out to second neighbors or 10 ions to the defect explicitly. Norgett[27] obtained results similar to ours in his calculations. Our semiclassical potential I gives somewhat lower absolute values than potential II for both anion vacancy and interstitial formation energies in CaF_2. The agreement with the experimental anion Frenkel pair-formation energy in CaF_2 is also poorer for potential I; in BaF_2, however, the agreement with experiment is excellent for both potentials III and IV. It is to be emphasized that our agreement with experiment using potential III is all the more striking because the interactions were not determined empirically.

The results of our calculation of the anion vacancy and anion interstitial migration energies for CaF_2 and BaF_2 are given in Table III. Again, several radii r_A were employed. Up to 592, 124, 596, 326, and 124 ions were included in region A for the vacancy (0, 0, 0), vacancy saddle-point $(\frac{1}{4}, 0, \frac{1}{4})$, interstitial (0, 0, $\frac{1}{2}$), interstitial saddle-point $(\frac{1}{4}, \frac{1}{4}, \frac{1}{2})$, and interstitialcy saddle-point (0.075, 0.075, 0.370) calculations, respectively. (The interstitialcy saddle point was found by mapping the path.) The activation energies reported were obtained by subtracting the appropriate formation energies obtained by the fitting procedure discussed previously (see Fig. 5). Agreement of activation energies to within 0.1 eV were typically obtained by comparison of the results from the fitting procedure with the results obtained by subtracting E_A values corresponding to regions containing approximately equal numbers of ions for stable and saddle-point positions for each potential and each mode of motion studied.

The agreement with experiment for F^- vacancy migration in CaF_2 is excellent for both potentials I and II. It is difficult to decide between the potentials on this basis alone. Good agreement with experiment in BaF_2 using both potentials III and IV for anion vacancy migration is also obtained.

Also in BaF_2, we obtain remarkable agreement with the F^- interstitial activation energy measured by Barsis and Taylor.[6] Our calculation of the F^- interstitial migration energy in BaF_2 for both potentials clearly shows the mechanism of anion migration in this substance to be the interstitialcy mechanism.

The situation in CaF_2 is unfortunately not so clear. We find the interstitialcy mechanism to be energetically favorable to the interstitial mechanism by ~0.7 eV for both potentials I and II. Our calculations therefore indicate that the same anion interstitial mechanism of migration should exist for both CaF_2 and BaF_2. Unfortunately the experimental results differ so widely from one another that no definite conclusion can be drawn. Chakravorty's[24] calculations are in qualitative agreement with the present work in that he also found the interstitialcy

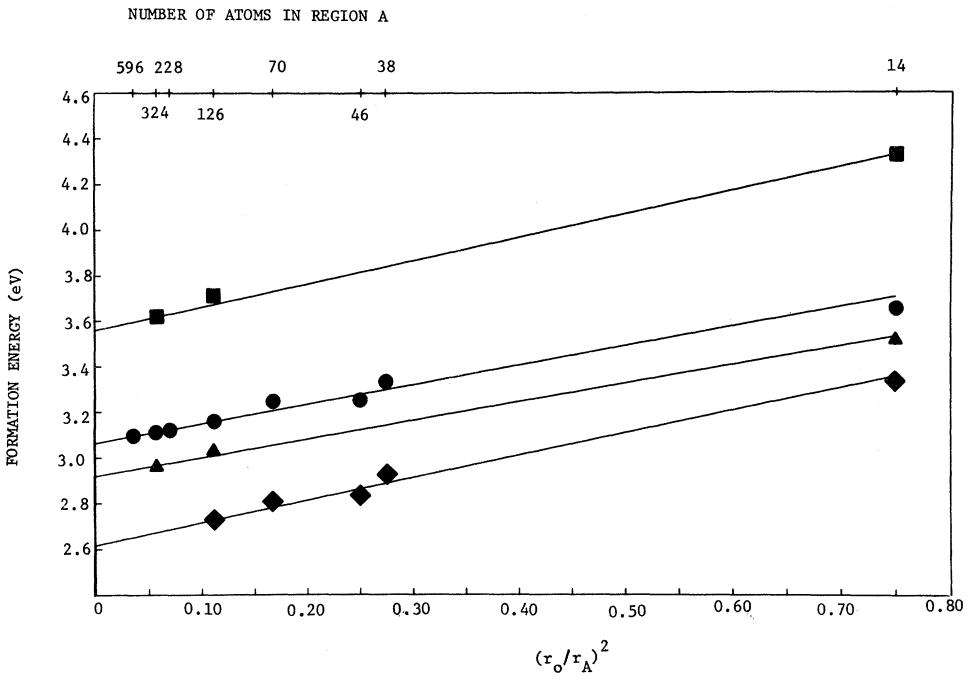

FIG. 6. Dependence of formation energy in eV on radius r_A of region A for an Ar atom at an interstice center in CaF_2. Straight line obtained from least-squares fit to energy values weighted by corresponding number of ions included in region A and are given at top of graph: ◆ present calculations using potential I; • present calculations using potential II; ■ Norgett calculations using potential FT (Ref. 27); ▲ Norgett calculations using potential A (Ref. 27).

mechanism to be favorable; however, each energy value is considerably greater than our results even though he employed the same potential (Franklin's[25] set number 3 potentials which are our potential II). If we compare his interstitialcy value with ours while allowing only 14 ions to be in region A, the number included by Chakravorty, we find they agree within ~0.07 eV, showing that his high-energy values are a consequence of using an insufficient number of ions in the immediate region surrounding the defect.

We have shown that the Born–Mayer potentials employed here and those obtained from the Wedepohl method give realistic formation and activation energies when used in the polarizable point-charge method utilized in this paper.

The important conclusion to be drawn from these calculations of the intrinsic defect formation energies is that interactions between approximately 100 nearest-neighbor ions must be treated explicitly in order to properly account for the symmetry of the defect; the energy coming from the region outside region A can then be treated by one of several continuum approaches. Also we found that the behavior of the formation energy E_A, corresponding to region A, for all of the charged-point defects studied was proportional to r_A^{-1}.

B. Rare-Gas Complexes in CaF_2

The rare-gas atoms are considered to possess no net charge when in the fluorite crystal. As such the presence of a rare-gas atom will produce no long-range polarization effects going like $1/r_A$ as we found arising from charged defects. Instead we find that the polarization energy goes like $1/r_A^2$ in agreement with elastic theory, and as a result we can obtain a converged formation energy for a neutral-rare-gas point defect by extrapolating to $r_A^{-2}=0$ the least-squares straight-line fit to several (nine or more, in general) calculated values of E_A vs r_A^{-2}.

Figure 6 contains the results of our calculations of the formation energies of Ar atoms at an interstice center (0, 0, $\frac{1}{2}$) plotted against r_A^{-2}, with the number of atoms included in region A given at the top of the figure; both potentials I and II were employed. Norgett's[27] calculated values for an Ar interstitial using his potentials A and FT are also plotted in Fig. 6. His calculated value for 324 atoms in region A (16 shells) gives a formation energy within 0.1 eV of the extrapolated value we obtain from his results.

In Fig. 7 we have plotted the calculated formation energies for Ar at the interstitial saddle point ($\frac{1}{4}$, $\frac{1}{4}$, $\frac{1}{2}$) vs r_A^{-2}. Here the close packing of the configuration requires the inclusion of a larger number of atoms in region A to obtain a converged value. Again Norgett's calculated values for Ar at the interstitial saddle point for both of his potentials are included. Note that in this case the 110 atom region A (22 shells) which he used gives a formation energy which we find is about 0.9 eV too high when the correct energy is obtained by an $r_A^{-2}=0$ extrapolation on the E_A vs r_A^{-2} plot.

Using the formation energies from the previous technique (like Figs. 6 and 7 for Ar with an $r_A^{-2}=0$ extrapolation) we obtain the results for potential II listed in Table IV for He, Ne, and Ar. The for-

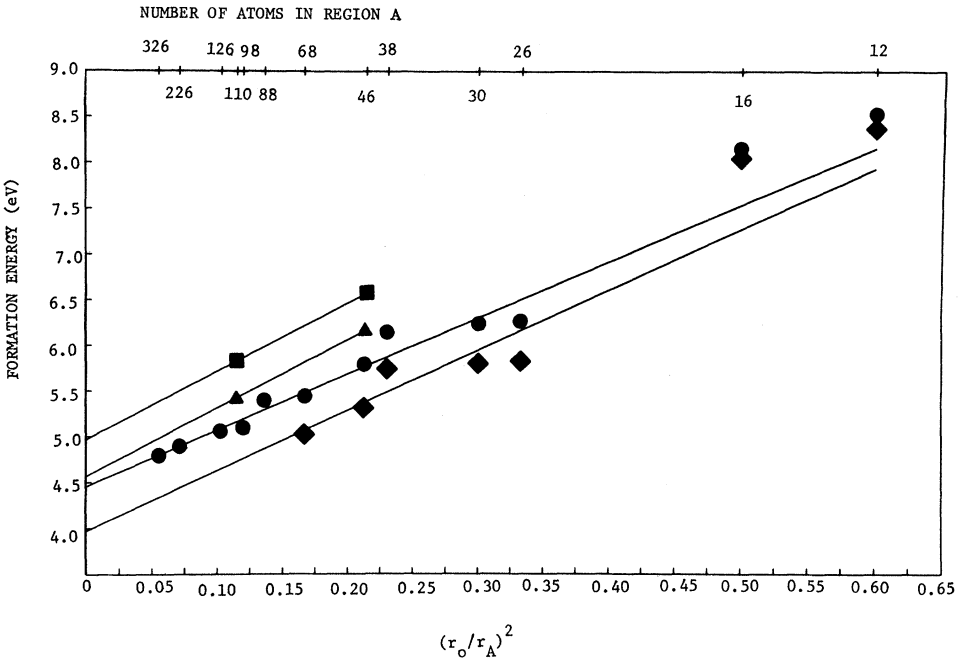

FIG. 7. Dependence of formation energy in eV on radius r_A of region A for an Ar atom at interstitial saddle point in CaF_2. Straight line obtained from least-squares fit to energy values weighted by corresponding number of ions included in region A and are given at top of graph: ◆ present calculations using potential I; • present calculations using potential II; ■ Norgett calculations using potential FT (Ref. 27); ▲ Norgett calculations using potential A (Ref. 27).

mation energies converge more slowly for increasing size of defect atom, as one might expect. The interstitial activation energies are near 1.4 eV for all three rare gases studied according to our calculations. From Figs. 6 and 7 the Ar interstitial migration energy for potential I is 1.30 eV, for Norgett's potential A it is 1.64 eV, and for potential FT it is 1.42 eV, the latter number being quite close to ours for potential II.

We also calculated the energy required to place a He, Ne, or Ar atom in an existing negative ion vacancy in CaF_2 using both potentials I and II. Just as for the vacancy alone, the calculated energies approach a straight line when plotted against r_A^{-1} for the larger values of r_A. The calculated formation energies for He in an anion vacancy for potentials I and II plotted against r_A^{-1} appear in Fig. 8 together with the best straight-line fits to the weighted values. As can be seen from Fig. 8, we are able to obtain an extrapolated value with a high degree of confidence using this technique. Our results listed in Table IV for all the rare gases studied indicates that it takes less energy to put a rare-gas atom in an existing negative ion vacancy than into an interstice. In addition, once in a negative ion vacancy it is prevented from moving to an interstitial site leaving behind a negative ion vacancy by about 1.7 eV for a He atom, 2.1 eV for a Ne atom, and 2.5 eV for an Ar atom.

Comparing our results with the experiments which have been performed,[28–37] we find that our calculated values for Ar moving by an interstitial mechanism are about one-half the experimental values ascribed to interstitial motion of 2.9–3.5 eV. Our values could be low but because our potentials I and II, in addition to Norgett's A and FT, give values which are close to one another when the proper formation energies are obtained (i.e., using the extrapolation technique shown for interstitial Ar in Figs. 6 and 7), the problem does not appear to be potential dependent. Another possibility is that the polarizable point-charge model is too over simplified, but the inclusion of additional terms (distortion dipole, van der Waals contributions, etc.) would not be expected to introduce the required 1.5

TABLE IV. Formation and activation energies in eV for rare-gas complexes in CaF_2 using potential II.

Rare-gas defect	He	Ne	Ar
Formation energy of rare gas at interstice center	0.49	1.59	3.08
Formation energy of rare gas at interstitial saddle point	1.80	3.05	4.45
Formation energy of rare gas in anion vacancy	4.40	5.10	6.45
Activation energy for interstitial motion	1.31	1.46	1.39
Energy to place rare gas in existing vacancy	0.25	0.95	2.30
Activation energy for substitutional detrapping from anion vacancy	1.7	2.1	2.5

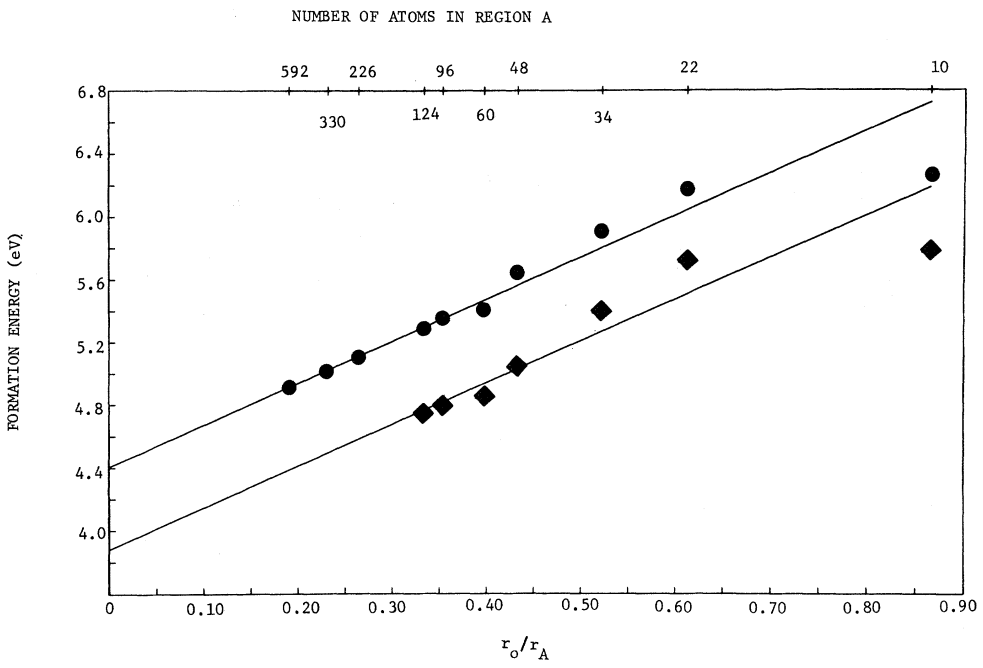

FIG. 8. Dependence of formation energy in eV on radius r_A of region A for a He atom in an F^- vacancy in CaF_2. Straight line obtained from least-squares fit to energy values weighted by corresponding number of ions included in region A and are given at top of graph: ◆ using potential I; ● using potential II.

eV or so to achieve agreement with experiment. Notice that the activation energy necessary to remove an Ar atom from an anion vacancy and put it at a stable interstice center is about 2.5 eV for potential II, from Table IV. This value is in agreement with the measured ones mentioned previously of 2.9–3.5 eV. Our feeling is that the measured "release" actually includes trapping such as would occur in vacancies, vacancy clusters, or impurities.

If another negative ion vacancy migrates next to a rare-gas atom in an anion vacancy our calculations indicate that the rare-gas atom can jump to the other negative ion vacancy with an activation energy of less than 0.1 eV for any of the three rare gases studied. Therefore, rare-gas motion by a negative ion vacancy mode will probably have as its rate controlling step the vacancy motion energy.

To summarize, we have shown that uncharged rare-gas defect complexes produce lattice polarization (ionic plus electronic) energy with a r_A^{-2} dependence and that one can get a converged formation energy value by a linear extrapolation to $r_A^{-2} = 0$ from several calculated values of E_A vs r_A^{-2}, with the largest region A comprising at least 100 atoms. We have also shown that the rare gases He, Ne, and Ar can move interstitially with an activation energy of about 1.4 eV and that a negative ion vacancy will trap these atoms with energies of 1.7, 2.1, and 2.5 eV for He, Ne, and Ar, respectively.

*Work supported by the U. S. Atomic Energy Commission.

[1]J. W. Twidel, J. Phys. Chem. Solids **31**, 299 (1970).
[2]H. Matzke, J. Mater. Sci. **5**, 831 (1970).
[3]V. V. Popov, Fiz. Tverd. Tela **11**, 1982 (1969) [Sov. Phys.-Solid State **11**, 1594 (1970)].
[4]J. H. Chen and M. S. McDonough, Phys. Rev. **185**, 453 (1969).
[5]T. I. Nikitinskaya *et al.*, Fiz. Tverd. Tela **9**, 2111 (1967) [Sov. Phys.-Solid State **9**, 1656 (1968)].
[6]E. Barsis and A. Taylor, J. Chem. Phys. **48**, 4362 (1968).
[7]E. Barsis and A. Taylor, J. Chem. Phys. **48**, 4357 (1968).
[8]F. K. Fong and M. A. Hiller, J. Phys. Chem. **71**, 2854 (1967).
[9]W. L. Fielder, NASA Technical Report No. TND 3816, p. 20, 1967 (unpublished).
[10]V. A. Arkhangelskaya *et al.*, Fiz. Tverd. Tela **9**, 687 (1967) [Sov. Phys.-Solid State **9**, 539 (1967)].
[11]V. A. Arkhangelskaya *et al.*, Fiz. Tverd. Tela **7**, 3682 (1965) [Sov. Phys.-Solid State **7**, 2976 (1966)].
[12]P. D. Southgate, J. Phys. Chem. Solids **27**, 1623 (1966).
[13]E. Barsis and A. Taylor, J. Chem. Phys. **45**, 1154 (1966).
[14]R. J. Lysiak and P. P. Mahendroo, J. Chem. Phys. **44**, 4025 (1966).
[15]B. Rossing, Ph.D. thesis (MIT, 1966) (unpublished).
[16]W. Clark and W. W. Warren, Jr., Phys. Lett. **21**, 614 (1966).
[17]J. A. Champion, Br. J. Appl. Phys. **16**, 805 (1965).
[18]R. W. Ure, Jr., J. Chem. Phys. **26**, 1363 (1957).
[19]W. Bollmann *et al.*, Phys. Status Solidi **2**, 157 (1970).
[20]G. A. Keig and R. L. Coble, J. Appl. Phys. **39**, 6090 (1968).
[21]P. Asadi, Phys. Status Solidi **20**, K55 (1967).
[22]V. V. Ratnam, Phys. Status Solidi **16**, 549 (1966).
[23]K. Tharmalingham, Philos. Mag. **23**, 1999 (1971).
[24]D. Chakravorty, J. Phys. Chem. Solids **32**, 1091 (1971).
[25]A. D. Franklin, J. Phys. Chem. Solids **29**, 823 (1968).
[26]A. D. Franklin, Brit. Ceram Soc. J. **9**, 15 (1965).
[27]M. J. Norgett, J. Phys. C **4**, 298 (1971).
[28]A. S. Ong and T. S. Elleman, J. Nucl. Mater. **42**, 191 (1972).
[29]F. W. Felix and S. Y. T. Lagerwall, Phys. Status Solidi **4**, 73 (1971).
[30]F. W. Felix and S. Y. T. Lagerwall, Phys. Status Solidi **33**, 85

(1969).
[31]J. Biersack and A. Brenner, Nukleonik **10**, 264 (1967).
[32]J. Biersack, Nukleonik **10**, 267 (1967).
[33]R. Kelly and Hj. Matzke, J. Nucl. Mater. **17**, 179 (1965).
[34]T. Lagerwall, Trans. Chalmers Univ. Tech. Goteborg No. 307, (unpublished).
[35]Hj. Matzke, J. Nucl. Mater. **11**, 344 (1964).
[36]T. Lagerwall, Nukleonik **6**, 179 (1964).
[37]T. Lagerwall, Nukleonik **4**, 158 (1962).
[38]P. T. Wedepohl, Proc. Phys. Soc. Lond. **92**, 79 (1967).
[39]W. D. Wilson and C. L. Bisson, Phys. Rev. B **3**, 3984 (1971).
[40]W. Witte and W. Wolfel, Rev. Mod. Phys. **30**, 51 (1958).
[41]C. Kittel, in *Introduction to Solid State Physics* (Wiley, New York, 1956), p. 571.
[42]R. D. Hatcher and G. J. Dienes, Phys. Rev. 134, A214 (1964).
[43]W. D. Wilson *et al.*, Phys. Rev. **184**, 844 (1969).
[44]J. R. Tessman *et al.*, Phys. Rev. **92**, 890 (1953).
[45]A. Dalgarno and A. E. Kingston, Proc. R. Soc. A **259**, 424 (1960).
[46]R. J. Quigley and T. P. Das, Phys. Rev. **164**, 1185 (1967).
[47]W. Jost, J. Chem. Phys. **1**, 466 (1933).
[48]O. Ra, J. Chem. Phys. **52**, 3765 (1970).
[49]T. E. Brackett and E. B. Brackett, J. Phys. Chem. **69**, 3611 (1965).
[50]R. W. G. Wyckoff, in *Crystal Structures* (Interscience, New York, 1963), 2nd ed., Vol. 1, p.241.

PHYSICAL REVIEW B VOLUME 7, NUMBER 2 15 JANUARY 1973

Normal and Oblique Optical Phonons in $RbClO_3$†

D. M. Hwang and S. A. Solin
The Department of Physics and The James Franck Institute, The University of Chicago, Chicago, Illinois 60637
(Received 13 July 1972)

The frequencies, polarizations (transverse or longitudinal), and symmetry species of the normal optical phonons in $RbClO_3$ (those which propagate parallel or perpendicular to the optic axis) have been determined from polarized Raman spectra. Using *only* the Raman data, the dielectric transition strengths, damping constants, and plasma frequencies of *all* of the polar phonons have been calculated. The room-temperature values of the static dielectric constants were found to be $\epsilon_0^{\parallel}=4.97\pm0.14$ and $\epsilon_0^{\perp}=5.17\pm0.11$. The directional dispersion of each of the oblique optical phonons (those which propagate at an acute angle to the optic axis) has been measured from the Raman data and calculated using the phenomenological coupled-harmonic-oscillator model of Onstott and Lucovsky. Agreement between theory and experiment was excellent. Infrared transmission spectra of mull samples have been recorded. The structural features of these spectra were found to be consistent with the polarized Raman data. Isotope splittings of some of the transverse optical phonons have been observed in both the Raman and infrared spectra and compared with the corresponding splittings of the chlorate-ion vibrational modes.

I. INTRODUCTION

Both $NaClO_3$ [1] and $KClO_3$ [2] have been the subject of a large number of optical investigations during the past several years. Most recently, Hartwig *et al.* carried out a thorough study of optical phonons in $NaClO_3$.[1] On the other hand, the chlorates of rubidium, lithium, and cesium have received little attention from optical spectroscopists and solid-state physicists in general.[3] The interest in $NaClO_3$ and $KClO_3$ is in part a manifestation of the ease with which these materials can be prepared as large optical quality single crystals.[4] To the contrary, $LiClO_3$ and $CsClO_3$ have to date defied preparation as nonpowdered single crystals, while we have only recently been successful in obtaining decent single crystals of $RbClO_3$.

There are a number of properties of rubidium chlorate which make it an interesting material, especially in comparison with $NaClO_3$ and $KClO_3$. It has a monomolecular five-atom rhombohedral primitive cell belonging to space-group symmetry C_{3v}^5 (R3m).[5] Thus, $RbClO_3$ is an ionic crystal with relatively high symmetry and, at the same time, very few optical modes. In contrast, $KClO_3$ has both low symmetry and two molecules per cell,[5] while $NaClO_3$ has high symmetry but four molecules per cell.[5] Like $NaClO_3$, $RbClO_3$ is piezoelectric but, in addition, is uniaxial. It has the unusual property that *all* of its Raman active phonons are polar and *all* of its polar phonons are Raman active. Therefore, $RbClO_3$ is an ideal crystal for examining the effects of both anisotropy forces and long-range electric forces on the directional dispersion of phonons.

It is well known that the interionic forces in the alkali chlorates are much weaker than the intraionic forces. Like a molecular crystal, the modes of $RbClO_3$ can be characterized as internal and external.[6] However, the internal modes exhibit no factor group splitting; there is a one-to-one correspondence between the vibrational modes of the free chlorate ion and the internal modes of $RbClO_3$. From a group-theoretical point of view then, $RbClO_3$ possesses a very basic and simple trigonal structure. Nevertheless, an analysis of the mixed